Fatigue of Welded Steel Structures
Due to Strong Earthquakes

II. Deteriorations of Welded Beam-to-Column Joints
Due to Low-Cycle Fatigue

By

Kiyoshi KANETA and Isao KOHZU

(Received June 30, 1981)

Abstract

This experiment was carried out from the viewpoint of evaluating the strength and the ductility of actual welded beam-to-column joints of steel structures in the event of earthquakes.

The experiment consisted of three features to reveal the abovementioned objectives; 1) a monotonic increasing load test to clarify the strength and toughness of steel plates stressed in the thickness direction, 2) a cyclic loading test to estimate the overall load-deflection characteristics and the energy absorbing capacity of the welded joint, and 3) a low-cycle fatigue test to gain a quantitative criterion of ductility requirement for the structural safety against earthquakes.

A special loading condition, that is, a bi-axial loading condition which contained the constant column axial force, was set up in order to examine whether or not a deterioration of the strength and the ductility would occur.

Anisotropy of the steel plates and a relatively poor deformation capacity of the welded joints were clearly observed from the results of the monotonic increasing load test with regard to some particular welding procedures.

A distinct fatigue strength deterioration of the welded joints is pointed out in comparison with that of the base metal, even though the energy absorbing capacity and the load-deflection relation do not differ from each other.

The presence of the constant column axial force does not influence the energy absorbing capacity or the fatigue strength of the welded beam-to-column joints.

1. Introduction

In the previous experiment[1], simple cyclic tests were carried out by using cylindrical specimens to clarify the cyclic load-deflection characteristics and low-cycle fatigue properties of welded joints in comparison with those of base metals.

It has been already reported by Prof. Naka[2] that anisotropy of hot rolled steel

---

Department of Architectural Engineering

plates has been observed between the rolling, transverse and thickness directions by the uni–axial loading tests on the butt–welded joints, and that it is necessary to pay more attention to the strength and toughness of the actual welded beam–to–column joints containing the steel plates stressed in the thickness directions.

Naka, Kato et al[3] reported that a detachable failure due to "lamellar tear" at the thickness direction occasionally occurred in the butt–welded joints because of a poor distortionability of the thick steel plates.

Ohji et al[4] made a test to clarify the distinctive difference of the low–cycle fatigue properties in three directions, using a special kind of metal. They reported that a remarkable deterioration of the fatigue strength was observed in the thickness directions.

In the actual cyclic loading of beam–to–column joints, consideration of such factors as a detachable failure and strain concentration phenomena is crucial for the aseismic design of steel buildings. Hence, it is necessary to estimate quantitatively the values for these characteristics through further experimental investigations.

For these reasons this paper deals with such experiments to find out the cyclic properties and the fatigue phenomena of welded beam–to–column joints made of 25 and 28mm thick steel plates, which configuration simulates those very often used in medium and high-rise steel buildings.

2. Procedure of the Experiments

2.1 Specimens

In the design of contemporary steel frames, the types of welded beam–to–column joints often used are as follows: The flanges of beams are connected with column flanges by means of butt welding, and the beam webs are either fillet welded (Fig. 2·1(a)) or bolted (Fig. 2·1(b)) together with the gusset plates welded on the column flanges as illustrated in Fig. 2·1.

In regard to the welded beam–to–column joints fabricated as described above, it is assumed in this paper that the flanges of the beam ends would be subjected to cyclic bending moments, and their webs would be subjected to shear forces. The specimens used were idealized models consisting of beam flanges (with the stress dominating in the rolling direction of the material), column flanges (thickness directions normal to rolling directions) and diaphragms (rolling directions) and their welded zones.

Three kinds of specimens, (namely, the base metal, A-, and B-type specimens) were used for the purpose of investigating the behaviors of the welded connections under uni–axial tension–compression loadings, simulating the cyclic bending moment fluctuation at the beam–ends in the event of an earthquake. Another kind of specimen (namely, C–type specimen) was used for the purpose of examining the influence of the constant column axial forces upon cyclic deformation properties of the welded joints,
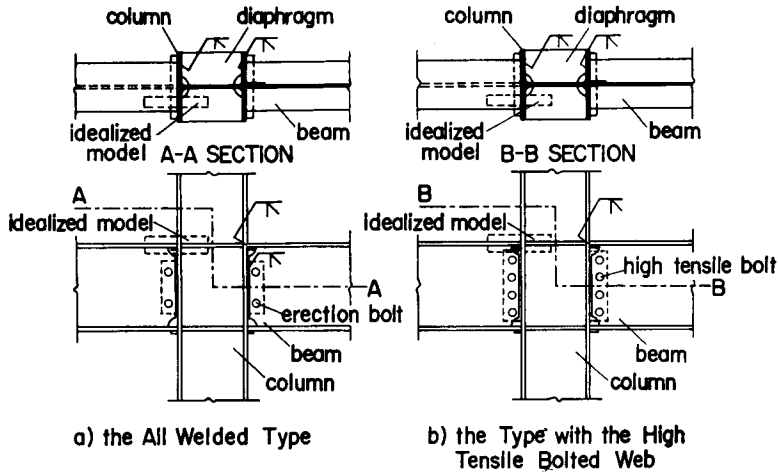
Fig. 2·1. Typical Welded Beam-to-Column Joints

such as occur in the inner beam–to–column joints of actual steel buildings. The welded specimens were classified into three types as follows;

a) A–type Specimens (flat plate type specimens)

The A–type specimens, together with the base metal specimens, had the shape and size as shown in Fig. 2·2.

b) B–type Specimens (cross–shaped specimens)

The column flanges of these specimens were relatively long (see Fig. 2·3) compared with those of the A–type specmiens. This was in order to examine the influence of the length of these column flanges upon the detachable failure of
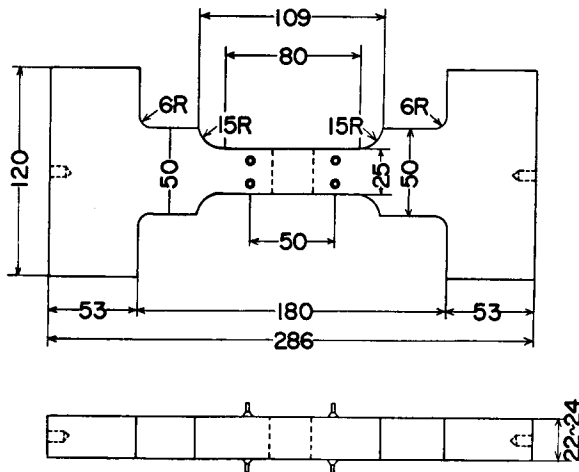
Fig. 2·2. A-Type Specimen (Unit: mm)
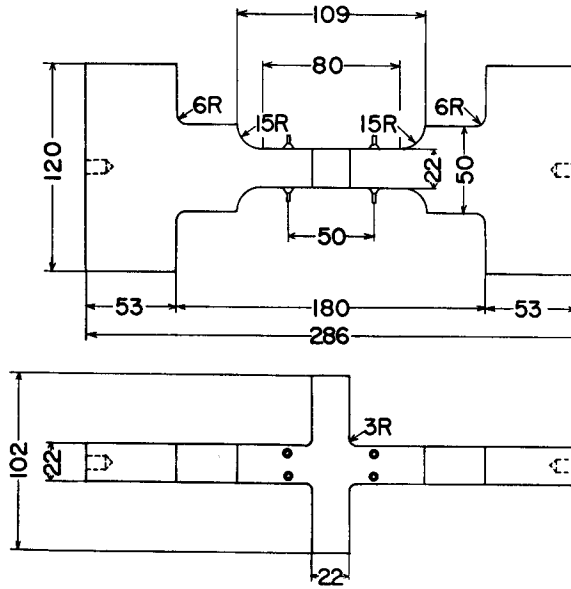
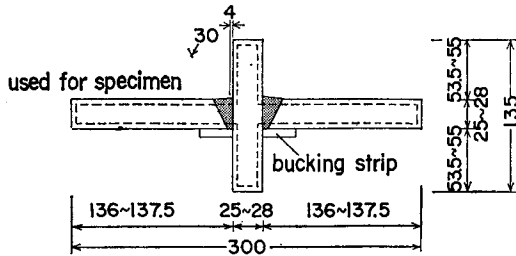Fig. 2·3. Specimen used for B-and C–Types (Unit: mm)

cut off flame cutting rolling direction

welding

50 130 ″ ″ ″ 130 50

750

rolling direction

15

used for specimen

bucking strip

136~137.5 25~28 136~137.5

300

53.5~55 53.5~55 25~28 135

Square Groove Welding

30 4

used for specimen

bucking strip

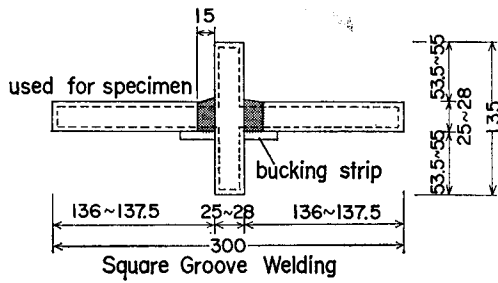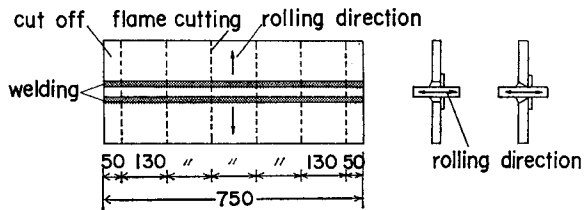136~137.5 25~28 136~137.5

300

53.5~55 53.5~55 25~28 135

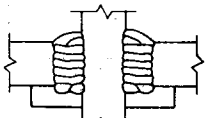Single Bevel Groove Welding
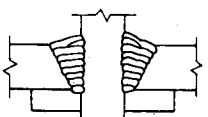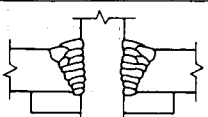
Fig. 2·4. Fabrication of Specimens (Unit: mm)
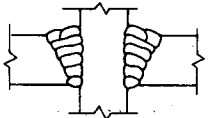
thick steel plates in comparison with the A–type specimens.

c) C–type specimens (cross–shaped specimens making allowance for constant column axial forces)

The specifications for the C–type specimens were the same as those for the B–type specimens, as shown in Fig. 2·3. However, since the aim of this experiment was to clarify whether or not any deterioration due to cyclic inelastic actions and plastic fatigue occurred as a result of the axial forces in the columns, the column flanges were subjected to constant column axial loads along the rolling directions and, furthermore, to cyclic tension–compression loads normal to column axial loads.

For the three types of specimens mentioned above, a series of fabrication and welding methods was executed, as illustrated in Figs. 2·4 and 5, in order to examine the influence of the different welding procedures upon cyclic deformation characteristics and fatigue properties. The welding process was either a CO_2–gas shielded arc butt welding or a "non–gas arc" butt welding. Two kinds of groove shapes were selected, namely, the single bevel groove and the square groove.

The base metals used for this experiment were JIS SS 41 steel plates, 25 and 28 mm thick. The chemical compositions of the plates were not always identical because of the differences in the specimens' lots. The mechanical properties and chemical

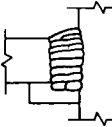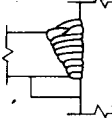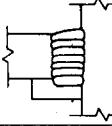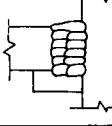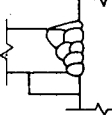| SERIES	WELDING PROCEDURE	GROOVE	SECTION	WELDING POSITION	PASS	CURRENT (A)	VOLTAGE (V)	WELDING WIRE
A – 1	CO_2 ARC WELDING WITH BACK RUN	SINGLE BEVEL GROOVE		FLAT	6 + 1	380	38	MG50 1.6ϕ
A – 2	CO_2 ARC WELDING WITH BACKING STRIP	SQUARE GROOVE		FLAT	9	320~380	37~40	MG50 1.6ϕ
A – 3	CO_2 ARC WELDING WITH BACKING STRIP	SINGLE BEVEL GROOVE		FLAT	9	320~370	36~40	MG50 1.6ϕ
A – 4	NON GAS SHIELDED ARC WELDING WITH BACKING STRIP	SINGLE BEVEL GROOVE		FLAT	10	400~450	20~25	OW56 3.2ϕ

SERIES	WELDING PROCEDURE	GROOVE	SECTION	WELDING POSITION	PASS	CURRENT (A)	VOLTAGE (V)	WELDING WIRE
B – 1 C – 1	CO_2 ARC WELDING WITH BACKING STRIP	SQUARE GROOVE		FLAT	10	330~380	38~40	MG50 1.6φ
B – 2 C – 2	CO_2 ARC WELDING WITH BACKING STRIP	SINGLE BEVEL GROOVE		FLAT	10	340~390	38~40	MG50 1.6φ
B – 3 C – 3	NON GAS SHIELDED ARC WELDING WITH BACKING STRIP	SQUARE GROOVE		FLAT	7	410~440	30~35	OW56 3.2φ
C – 4	CO_2 ARC WELDING WITH BACKING STRIP	SQUARE GROOVE		FLAT	11	320~380	36~40	MG50 1.6φ
C – 5	NON GAS SHIELDED ARC WELDING WITH BACKING STRIP	SINGLE BEVEL GROOVE		FLAT	7	420~450	32~35	OW56 3.2φ

Fig. 2·5. Welding Processes

Table 2·1. Material Properties obtained from the Mill Sheet

			A–1	A–2~4 B–1, 2 C–1, 2	B–3 C–3~5
Mechanical Properties	σ_y: Yield Point σ_u: Tensile Strength δ : Elongation	(kg/mm²) (kg/mm²) (%)	26 46 25	27 43 28	
Chemical Composition (%)		C Si Mn P S	0.16 0.04 1.07 0.011 0.017	0.17 0.20 0.70 0.014 0.014	

compositions of the base metals used for each type of specimen are tabulated in Table 2·1. As described in the previous experiment[1], the classification of each zone, namely the base metal, the weld metal and the heat affected zone, of the welded joints was done using a solution of nitric acid, the results of which are illustrated in Fig. 2·6.

2.2 Monotonic Loading Tests

A universal hydraulic testing machine with a loading capacity of 30 tons was used for
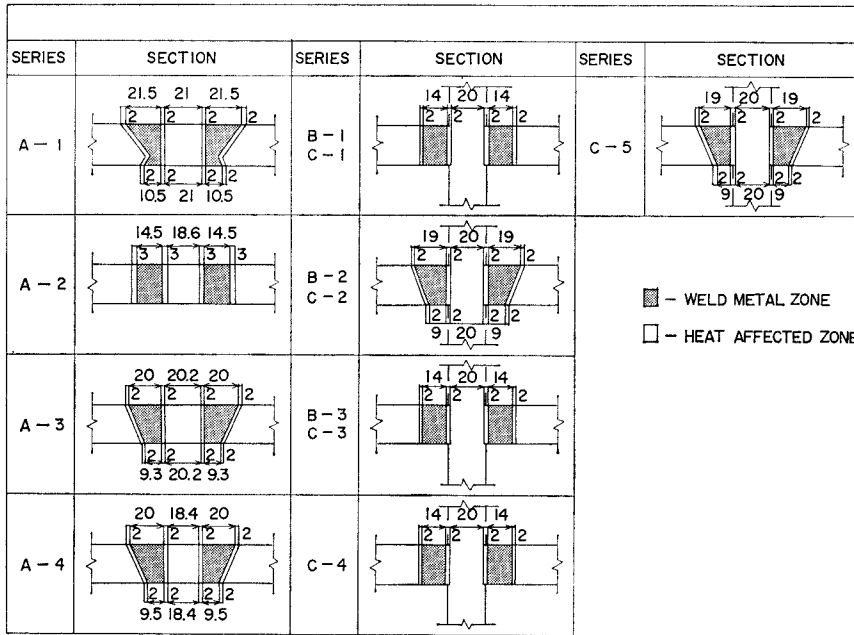
Fig. 2·6. Weld Metal and Heat Affected Zones (Unit: mm)

the three types of specimens and base metals in a quasistatic state. Fig. 2·7 shows the dimensions and the shape of the base metal specimen used for all A– and some B– and C–type specimens. Fig. 2·8 shows the dimensions and the shape used for the remaining B– and C–type specimens. The specimens were loaded in a longitudinal direction, and a continuous load-strain record was kept until failure on an X–Y recorder with the main strain outputs at the column flanges. Furthermore, the output at other points was measured and recorded by a high–speed multichannel strainmeter with additional plastic strain gauges mounted on the specimens, as illustrated in Fig. 2·9.
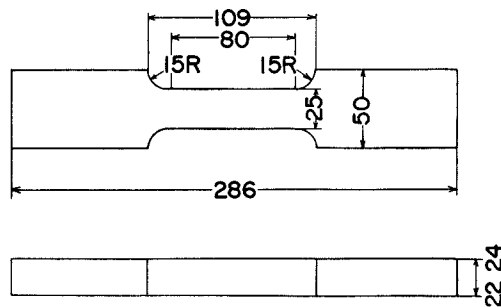

Fig. 2·7. Base Metal Specimen used for Monotonic Increasing Load Test (Unit: mm)
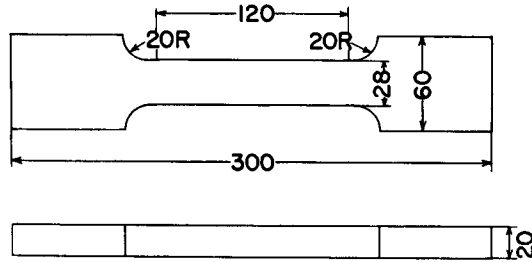
Fig. 2·8. Base Metal Specimen used for Monotonic Increasing Load Test (Unit: mm)

SERIES	GAUGE POSITIONS	SERIES	GAUGE POSITIONS
A – 1		B – 2 C – 2,5	
A – 2			
A – 3,4			
B – 1,3 C–1,3,4			

Fig. 2·9. Strain Gauge Positions

2.3 Cyclic Tests

There are two significant points to clarify in regard to cyclic inelastic actions and the low–cycle fatigue strength of welded joints. One is to clarify the general cyclic load–deflection relationships and low–cycle fatigue lives of welded joints. The other is to investigate in detail the development of strain at several specimen zones, and the influence of this strain behavior upon the deflection phenomenon as a whole. For the former objective, a pair of extensometers was fastened to the specimen by two sets of four small bolts that had been welded to the specimen surface. (See Fig. 2·10) For the latter objective, several plastic strain gauges were mounted on the specimen zones in the same way as for monotonic increasing load tests. (See Fig. 2·9).
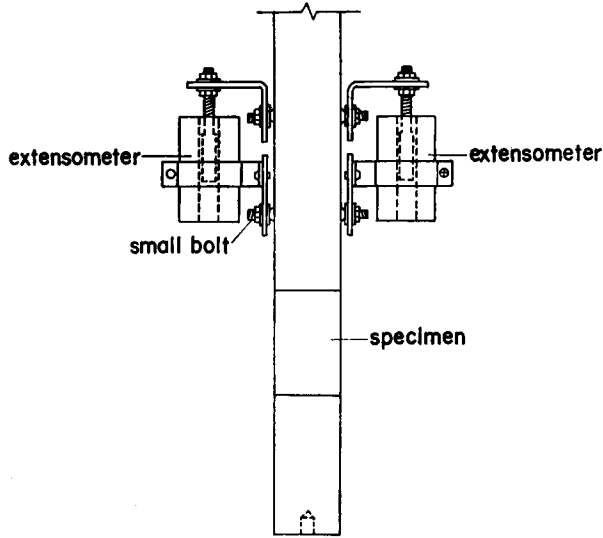
Fig. 2·10.   Set-up of Extensometers
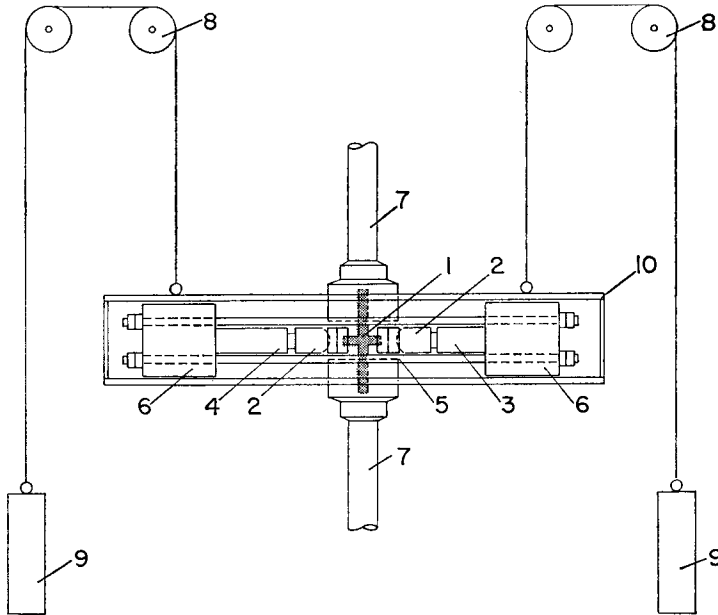
1	SPECIMEN	6	RIGID BEAM
2	PIN JOINT	7	PULL ROD (AUTOGRAPH)
3	HYDRAULIC JACK	8	PULLY
4	TRANSDUCER	9	COUNTER-WEIGHT
5	PC BAR	10	GUIDE FRAME

Fig. 2·11.   Special Loading Apparatus for C-Type Specimens

A 50–ton capacity universal testing machine, "autograph", was used to load the specimens cyclically. The tension–compression load was measured by a transducer mounted on the cross–head of the reaction frame. Further, certain designated distortion amplitudes were monitored by the above mentioned extensometers. The distortion–versus–load was recorded continuously until a failure on an X–Y recorder attached to the control equipment of the autograph.

Every specimen in cyclic tests was repeatedly loaded at a certain select constant distortion amplitude in the average elasto–plasto strain range between ± 0.5 and ± 2.08 %, that is, ± 0.25 and ± 1.04 mm distortion for the 5.0 cm gauge length.

The C–type specimens were also subjected to the additional loading of a constant column force. In order to supply the constant column axial force, a special counterbalanced loading apparatus was devised as shown in Fig. 2·11. This apparatus was attached to the counter–weights by wires slung through pulleys being fastened to a rigid beam bolted on the top of the reaction frame of the autograph. The load directions are schematically shown in Fig. 2· 12.
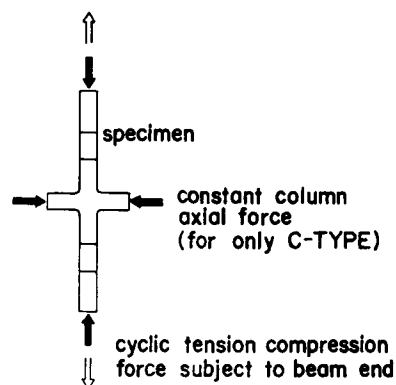
The constant axial load was selected in the range from 0.2 to 0.6 times the column yield strength of the column flange.

Fig. 2·12. Loading Condition for C–Type Specimens

3. Results of the Experiment

3.1 Monotonic Increasing Load

The results for three kinds of base metals are summarized in Table 2·2. The test results are somewhat different from those in the mill sheet. Similar monotonic increasing load tests were also carried out for the welded joints of the A–, B– and C–type

Table 2·2. Results of Monotonic Increasing Load Tests of Base Metals

|		A–1	A–2~4 B–1,2 C–1,2	B–3 C–3~5
σ_y: Yield Point	(kg/mm²)	24.9	24.9	22.4
ε_y: Yield Strain	(%)	0.12	0.11	0.13
σ_u: Tensile Strength	(kg/mm²)	44.4	42.8	43.8
δ^*: Elongation	(%)	33	33	39
ϕ: Reduction of Area	(%)	67	66	59
ε_f: Monotonic True Fracture Ductility		1.11	1.08	0.89

*: gauge length 50mm

Table 2·3. Results of Monotonic Increasing Load Tests of Welded Joints

			A-1	A-2	A-3	A-4	B-1	B-2	C-5
σ_u:	Tensile Strength	(kg/mm²)	44.2	47.3	47.7	46.3	47.8**	48.4**	——
δ*:	Elongation	(%)	7.8	11.0	11.0	3.5	——	——	——
ϕ :	Reduction of Area	(%)	10.7	32.0	24.0	8.0	——	——	——
ε_f:	Monotonic True Fracture Ductility		0.11	0.39	0.27	0.08	——	——	0.15

*: gauge length 50mm
**: fractured at the
    location of base
    metal

specimens. These results are tabulated in Table 2·3. In spite of the ample ductility of the base metals, a brittle fracture with little reduction of the cross sectional area at the column flange sections was observed in the A-type specimens. This tendency was especially remarkable for the A-4 type specimens assembled by means of non–gas welding.

Fig. 2·13 (a) ∼(c) shows the nominal stress–strain relationships at the column flanges and the weld metal zones for the A-type specimens, in comparison with those of the base metals. It should be noted from these figures that the proportional limits measured at the column flanges and the weld metals are much higher than the yield points of the base metals. Moreover, a remarkable reduction in ductility was evidenced by the strain at the fracture points, as compared with those of the base metals. These strains were about 7.5, 9.0, 15.0 and 5.0 % for the A-1∼4 type specimens, respecti-
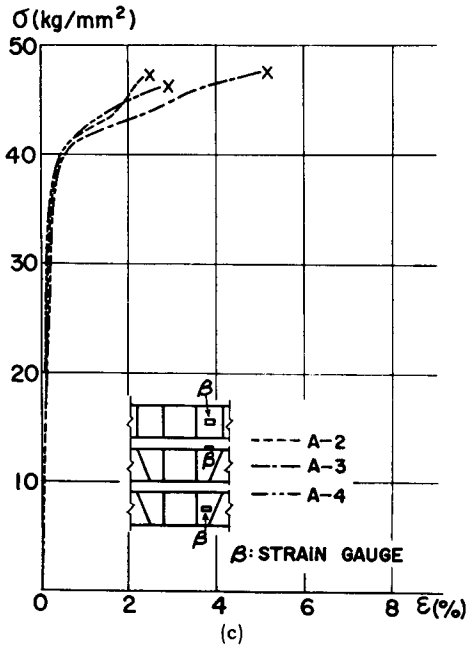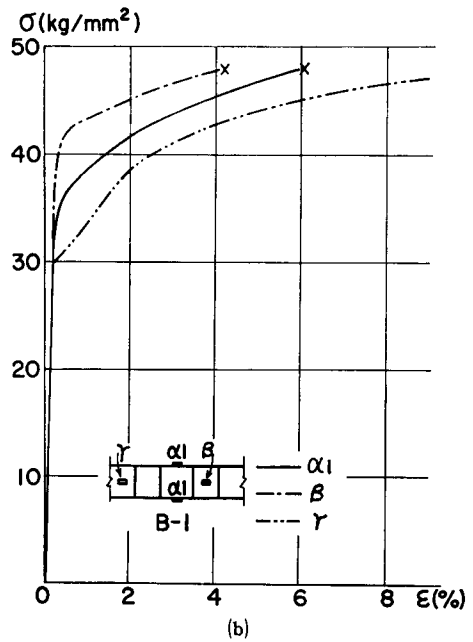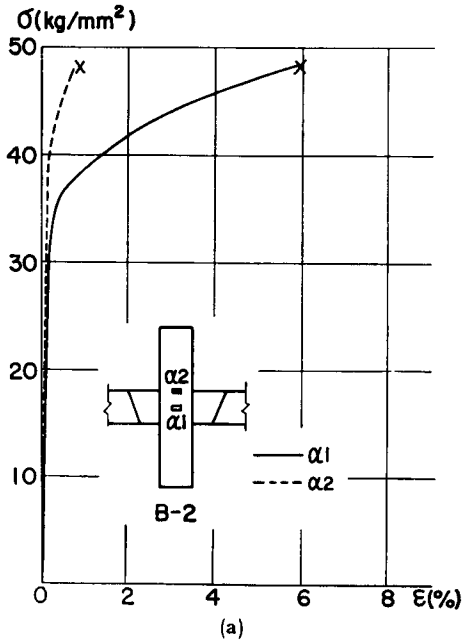

(a)

(b)
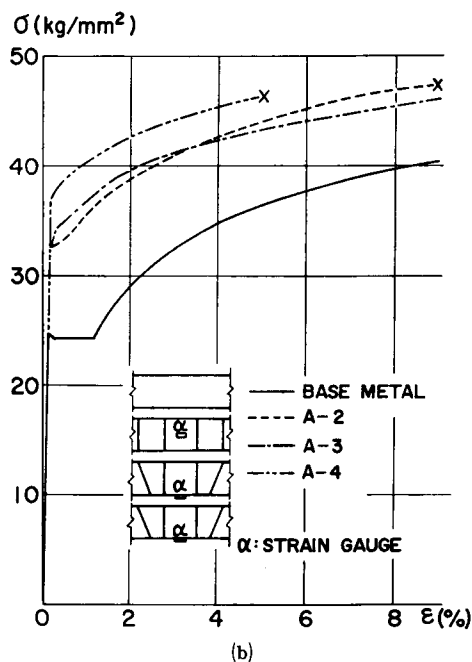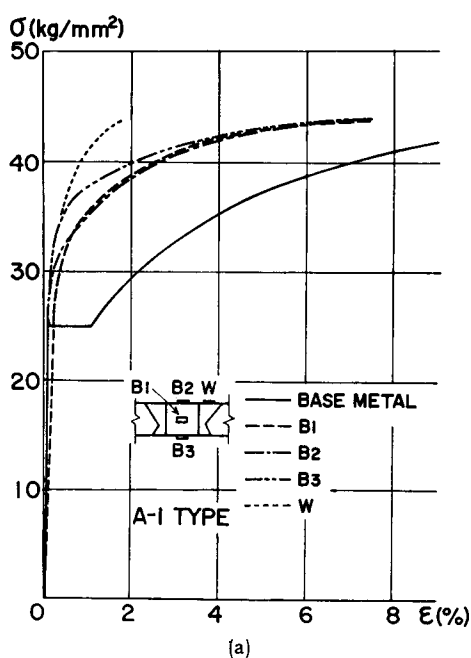
Fig. 2·13. Monotonic Stress–Strain Relations of A–Type Specimens

vely.

However, in similar experiments conducted by using specimens with comparatively long column flanges, namely, the B–1 and B–2 type specimens, it was observed that failure occurred at locations on the beam flanges (or diaphragms) which were far
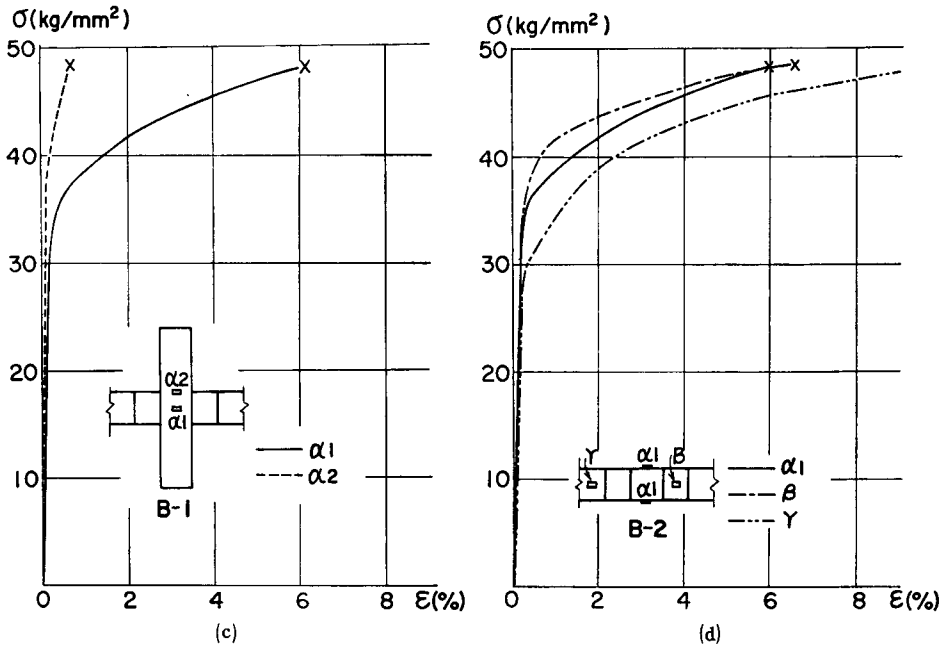
Fig. 2·14. Monotonic Stress-Strain Relations of B-Type Specimens

away from the column flanges, although the latter parts showed poor plastic deforma-
tion properties, as shown in Fig. 2·14, (a)∼(d).

3.2 Results of Cyclic Tests Based on Load-Deflection Relationships

Figs. 2·15∼17 show typical examples of hysteresis loops from the initial states to
several cycles later, for the base metals and the three types of welded joints. From the
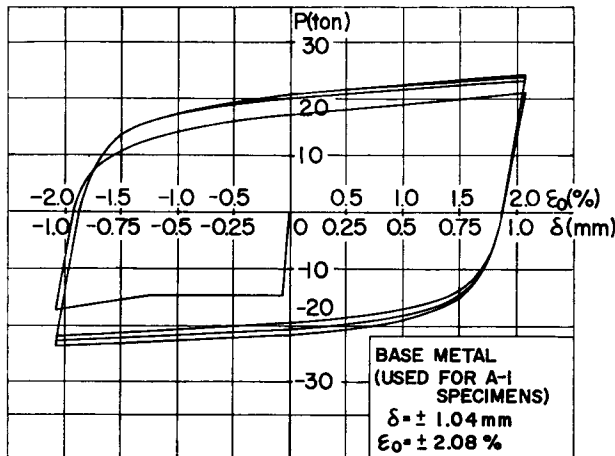figure for base metal (Fig. 2·15), the following phenomena were apparent. Distinct

Fig. 2·15. Load-Deflection Curves of Base Metals at the Initial Few Cycles
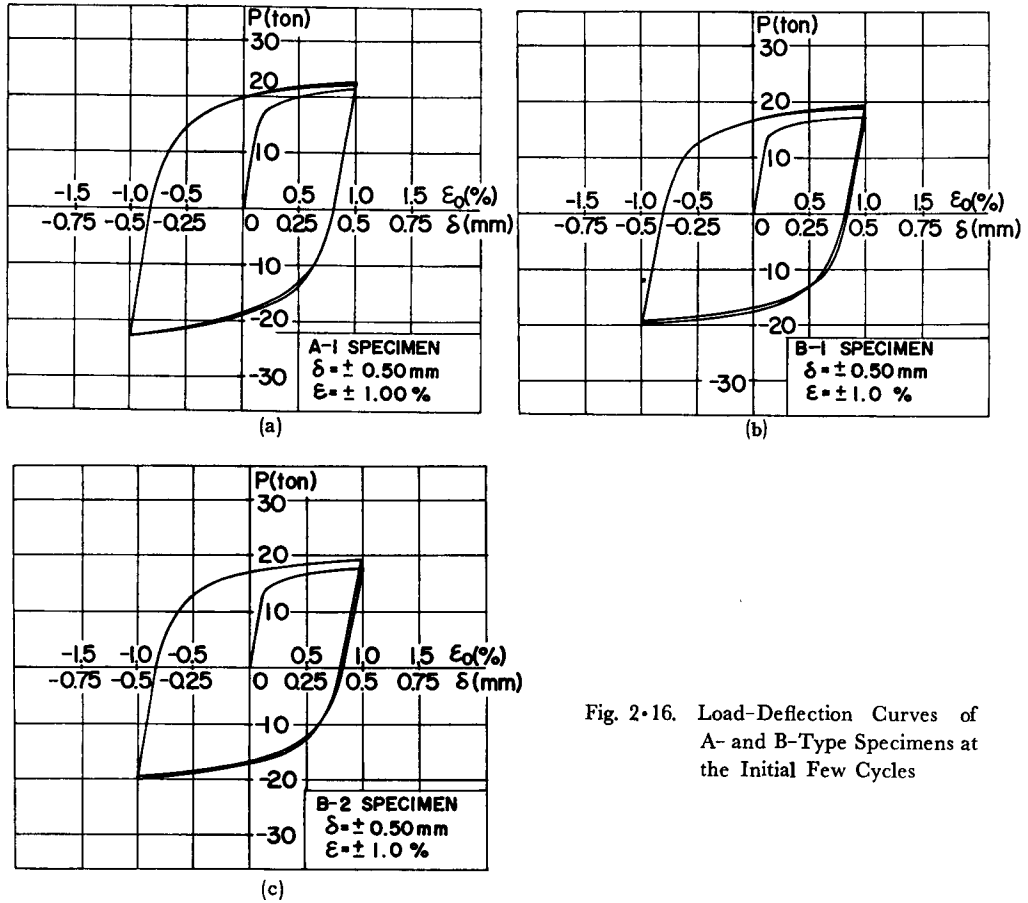
(a)

(b)

(c)

Fig. 2·16.   Load–Deflection Curves of
A– and B–Type Specimens at
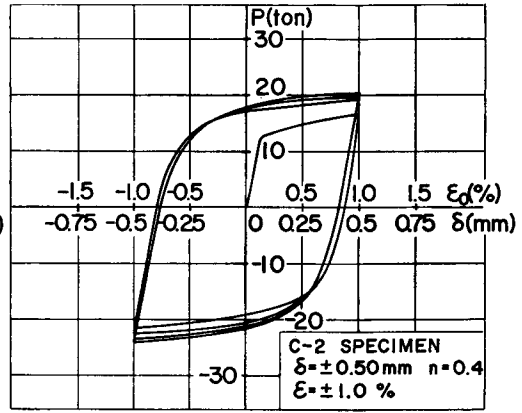the Initial Few Cycles

yield points existed in the virgin state, and strain hardening was initiated at about 1.2
% strain. The so–called Bauschinger effect can be observed to occur after the loads
were reversed from the initial peak loads. At the opposite side of the initial excursion,
the peak load exhibited a remarkable increase. Further, the gradual increase of peak
loads continued to occur in the subsequent excursions, that is, the so–called cyclic
hardening phenomena were observed.

On the other hand, the behavior of specimens consisting of welded joints did not
indicate the existence of any distinct yield points. In particular, for the A– and B–type
specimens, the peak load tended to converge rapidly upon a constant value after the
initial excursion occurred. (See Fig. 2·16(a)∼(c)). However, in the case of the C–
type specimens, as in the case of the base metals, a gradual increase of peak load was
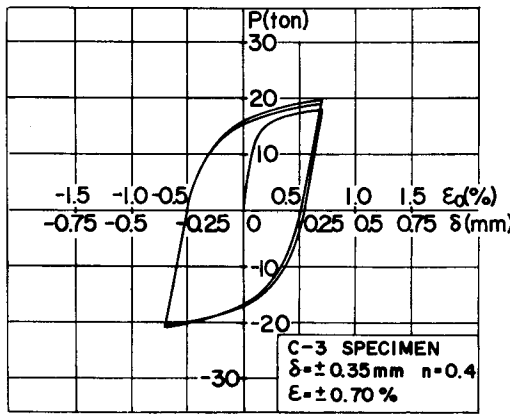evident, as shown in Fig. 2·17(a)∼(e).

Further, in comparison with the results of the cyclic tests using the B–type speci-
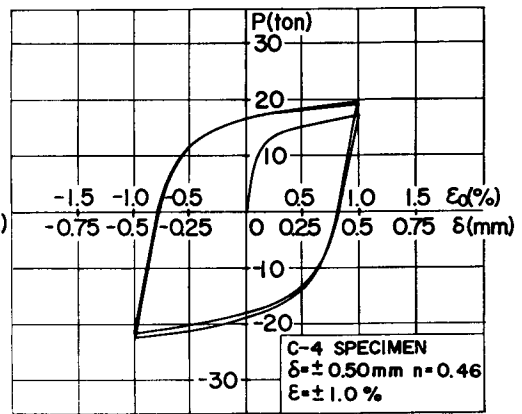mens, the proportional limit load at the initial state became smaller as the value of the
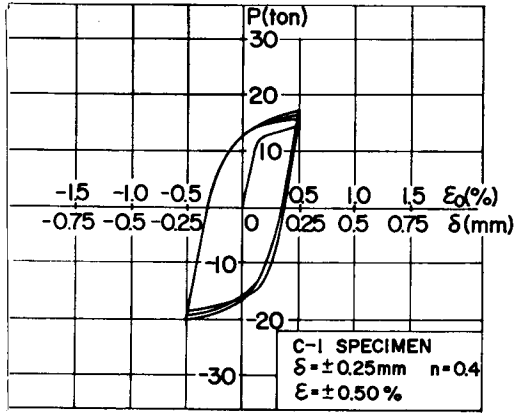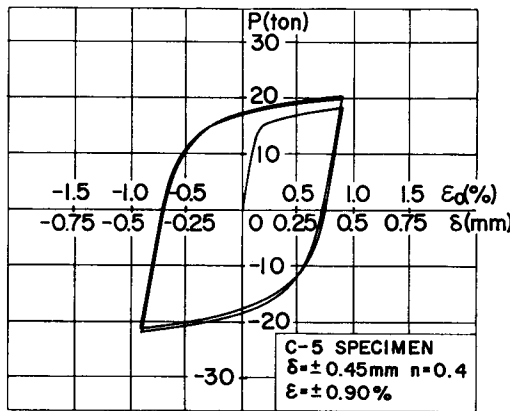
(a)

(b)

(c)

(d)

(e)

Fig. 2·17.   Load–Deflection Curves of C–Type Specimens at the Initial Few Cycles

constant column axial force became larger. Specifically, the peak loads at the compression side enlarged, that is, the hysteresis loops, in comparison with those of B–type specimens, moved downward parallel to the P–axis of the P–δ diagrams. (See Fig. 2· 17(a)∼(e)).

From the results of the welded joints, it may be said that there were no apparent distinctions between different welding procedures or groove shapes.

For the three types of specimens, the peak loads were stabilized after the initial few cycles at constant values, or decreased very slightly over the greater part of their lives. At the final stages, the peak loads fell suddenly, without any appearance of cracks, as in the case of the A–type specimens. In the cases of the other specimens, after the appearance and growth of cracks were observed in later lives, especially at the column flanges (near the heat–affected zones), the peak loads at the tension sides decreased gradually and the specimens fractured.

Some specimens, belonging to the B–type which were loaded at larger distortion amplitudes, as well as the C–type specimens with higher column flange forces showed a local buckling behavior during the cyclic loadings. However, these hysteresis loops were stable, and no degrading was observed.

3.3 Results of Strain Behaviors during Cyclic Tests

a) A– and B–type specimens

As the welded specimens used in this experiment consisted of materials with different mechanical properties, the local cyclic strain behaviors were somewhat different. At the initial stages of the cyclic loading, the output of the strain measurements showed certain distinct features. The strain values of the column flanges and the beam flanges (or the diaphragms) were remarkably large in comparison with those of the welded zones.   (See Fig. 2·18(a)∼(d)). After several loading cycles, the strain ranges

(a)
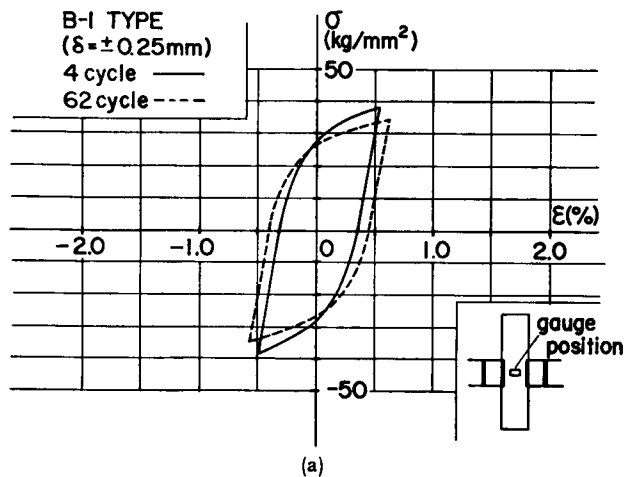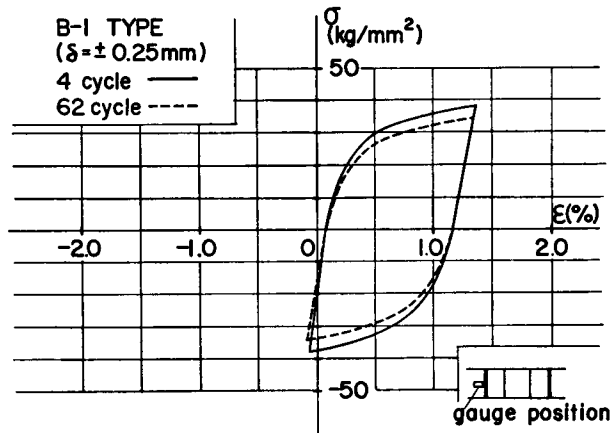
(b)
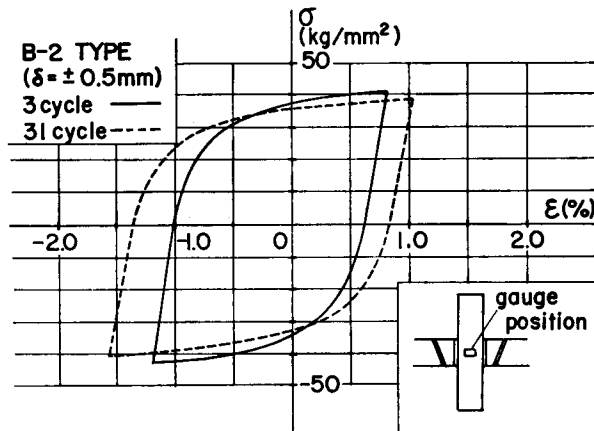
(c)

(d)

Fig. 2·18. Stress–Strain Relations at the Beam and the Column
Flanges of B-Type Specimens.
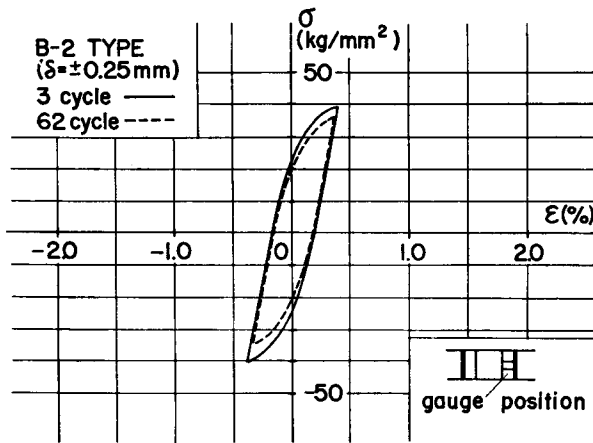
Fig. 2·19. Stress-Strain Relation at the Welded Zone of B-Type Specimen

of the column flanges increased gradually, whereas those of the beam flanges (or the diaphragms) decreased or remained constant. The strain values of the welded zones, however, showed little or no variation. (See Fig. 2·19).

b) C-type specimens

At the initial stages, the strain values of the column flanges showed predominantly high values and, at the same time, tended to shift toward the tension side. In contrast, the strain values of the beam flanges (or the diaphragms) tended to drift to the compression sides. (See Fig. 2·20). Such phenomena may well explain the local buckling behaviors during cyclic loadings.
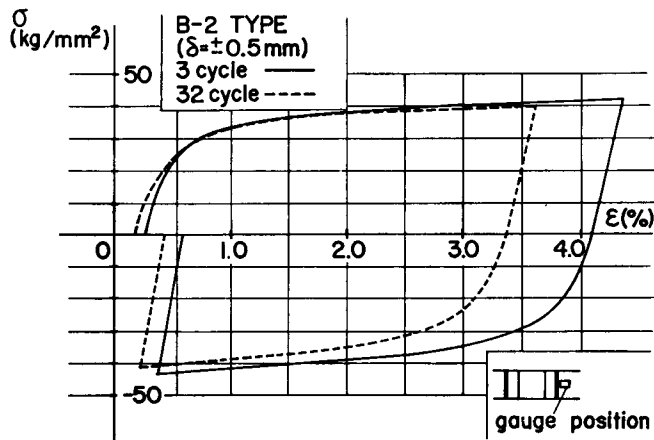

Fig. 2·20. Stress-Strain Relations at the Beam and the Column Flanges of C-Type Specimen

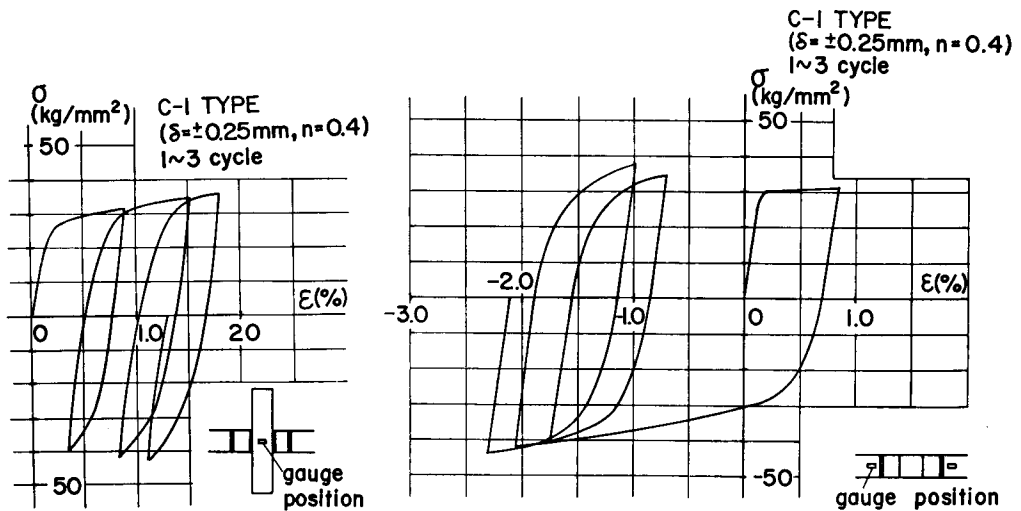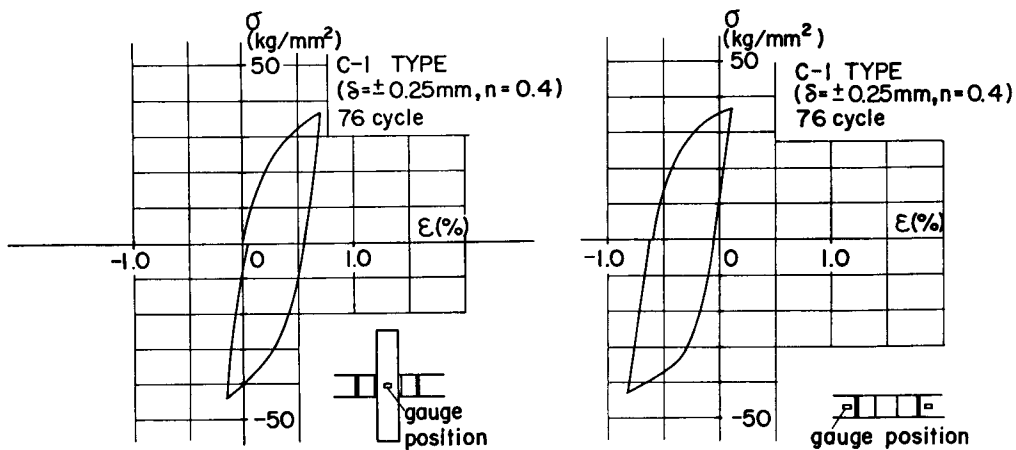Fig. 2·21.   Stress–Strain Relations at the Beam and the Column Flanges
of C–Type Specimen at the Steady State
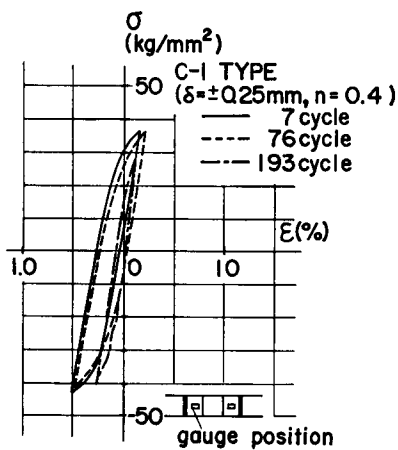
Fig. 2·22.   Stress–Strain Relation
at the Welded Zone of
C–Type Specimen

After many cycles, the strain values of the beam flanges (or the diaphragms) and the column flanges tended to converge and stabilize, as shown in Fig. 2·21. However, the strain values of the weld metals remained unchanged throughout the duration of their lives. (Fig. 2·22)

4.   Considerations

4.1   Yield Distortion

It is covenient for practical purposes to formulate the initial and the "cyclic load–plastic deflection" curves. These can be drawn by connecting the peak loads and the correspondent plastic distortion amplitudes, and then estimate the fatigue strength in the non–dimensional form as suggested in Ref. 1.

Each yield distortion ε_{y0} can be determined by defining the distortion at the lower yield point in the case of the base metal.

For the A– and B–type specimens, the non–dimensional elastic and plastic distortion amplitudes can be calculated by dividing those values by the yield distortion ε_{y0}. The yield distortion for each specimen was obtained by referring to the load–strain relation at the column flange in the thickness direction at the initial cycle. Since a 0. 2 % offset strain ε_y at the column flange was obtainable from the load–strain curve, the yield

distortion ε_{y0} could be defined as the distortion at the point where the load arrives at the 0.2 % off-set strain in the thickness direction ε_y. This is because all specimens fractured near the heat affected zones of the column flange in the thickness direction.

In the case of the C-type specimen, it is necessary to compute the yield distortion ε_{y0} by taking into consideration the bi-axial loading conditions. As is apparent from the monotonic increasing load tests on this mild steel, it can be concluded that the aniso-tropy exists between the rolling direction and the thickness direction. Therefore, the yield stress in the thickness direction Z must be computed first, incorporating a yield criterion by taking into consideration the anisotropic property. This can be derived from the column axial stress σ_x expressing the stress in the rolling direction of the plate, and from the nominal yield stress at the initial state σ_x that can be obtained from the 0.12 % off-set strain in the thickness direction.

As reported by Prof. Naka[2], some hot rolled steel plates show anisotropy in the rolling, transverse and thickness directions. However, as no significant difference be-tween the mechanical properties of the rolling and transverse directions can be obser-ved from the test results of Refs. 2 and 4, it could be assumed that the distinct difference exists only in the mechanical properties of the thickness direction.

The yield criterion is assumed to follow a method proposed by Hill[5], and the following equation,

$$F(\sigma_y-\sigma_z)^2+G(\sigma_z-\sigma_x)^2+H(\sigma_x-\sigma_y)^2+2L\tau_{yz}^2+2M\tau_{zx}^2+2N\tau_{xy}^2=1 \tag{1}$$

where F, G, H, L, M and N are parameters being characteristic of the current state of anisotropy.

From the results of this experiment, we can say that the terms τ_{yz}, τ_{zx} and τ_{xy} can be equalized to zero. Let X, Y and Z denote the yield stresses in the uni-axial state in the rolling, transverse and thickness directions, respectively. Moreover, let X be equal to Y, and the following equations can be written:

$$2F=2G=\frac{1}{Z^2}$$

$$H=\frac{1}{X^2}-\frac{1}{2Z^2} \tag{2}$$

Substituting Eq. (1) into Eq. (2), we have

$$\frac{\sigma_z^2}{2Z^2}+\frac{1}{2Z^2}(\sigma_z-\sigma_x)^2+\left(\frac{1}{X^2}-\frac{1}{2Z^2}\right)\cdot\sigma_x^2=1 \tag{3}$$

From Eq. (3), Z can be solved in the following form:

$$Z=\sqrt{\frac{\sigma_x\cdot(\sigma_x-\sigma_z)\cdot X^2}{X^2-\sigma_x^2}}$$

Since the value X has been obtained from the results of the monotonic increasing load tests, the value Z for each C-type specimen can be calculated by also using the experimental values, σ_x and σ_z.

Thus, the yield distortion ε_{yo} can be obtained using the relation between σ_z and its corresponding distortion, and the above-mentioned value Z.

4.2 Stress-Strain Relationships at the Initial State and Steady State for Base Metals and A- and B-type Specimens

It is evident from Fig. 2·15 and 16 that there is a difference in the shapes of the load–deflection curves between the initial state and the steady state. For this reason, it is necessary to sort the load-deflection curves into two cases, namely, those of the initial state and of the steady–state.

a) Initial State

The plots of the load and the corresponding plastic deflections for the base metals can be drawn as two straight lines on a log–log scale, as shown in Fig. 2·23(a): In contrast, in the case of the A- and B-type specimens, the test results can be plotted
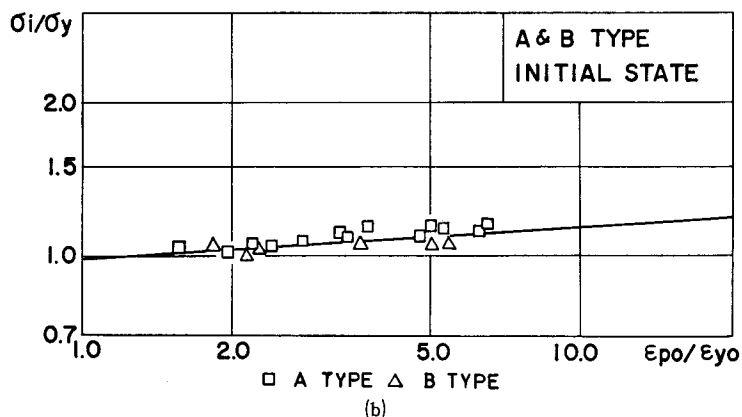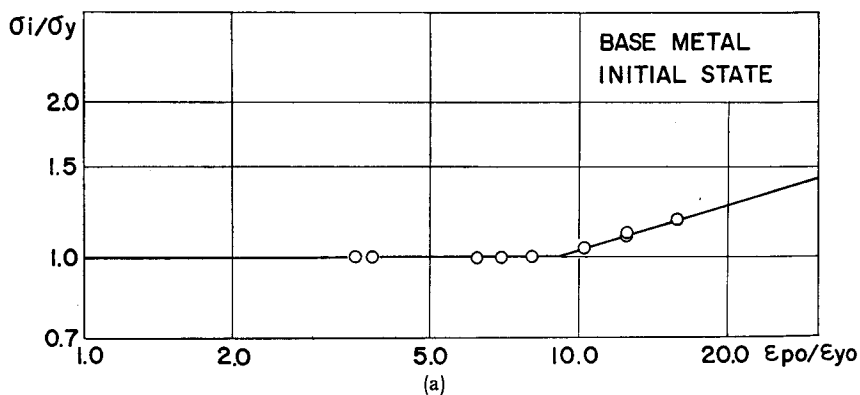

(a)

(b)

Fig. 2·23. Non-dimensional Stress and Plastic Distortion Relations at the Initial State

on one straight line. (See Fig. 2·23(b)). That is, the welded joints do not show the distinctive plastic flow or behave as strain–hardening material within the inelastic range.

Applying the least mean–square method, these relations can be formulated as follows:

For the base metal within the range of strain hardening:

$$\frac{\sigma_i}{\sigma_y} = 0.54 \cdot \left(\frac{\varepsilon_{p0}}{\varepsilon_{y0}}\right)^{0.29} \tag{5}$$

For the A– and B–type specimens:

$$\frac{\sigma_i}{\sigma_y} = 0.99 \cdot \left(\frac{\varepsilon_{p0}}{\varepsilon_{y0}}\right)^{0.064} \tag{6}$$

b) Steady State

The cyclic stress-strain curves proposed by Morrow, as reported in Ref. 1, are convenient for comparing the characteristics of the stress-strain curves with each other for many types of base metals and the welded joints. As in the case of the initial state, the peak stress σ_s/σ_y and the corresponding plastic average distortion amplitude $\varepsilon_{p0}/\varepsilon_{y0}$ in the non–dimensional form, were plotted as shown in Fig. 2·24(a) and (b).

Since each set of these data as plotted on the log-log scale accurately shows the linearity in respect to its corresponding figure, the linear regressions method could be applied as a first approximation. Each equation can be formulated as follows:

For the base metal:

$$\frac{\sigma_s}{\sigma_y} = 0.97 \cdot \left(\frac{\varepsilon_{p0}}{\varepsilon_{y0}}\right)^{0.19} \tag{7}$$

For the A– and B–type specimens:

$$\frac{\sigma_s}{\sigma_y} = 0.87 \cdot \left(\frac{\varepsilon_{p0}}{\varepsilon_{y0}}\right)^{0.17} \tag{8}$$

(a)
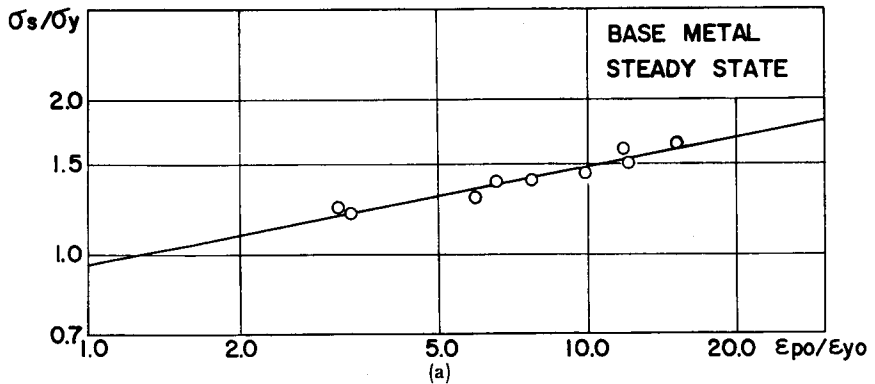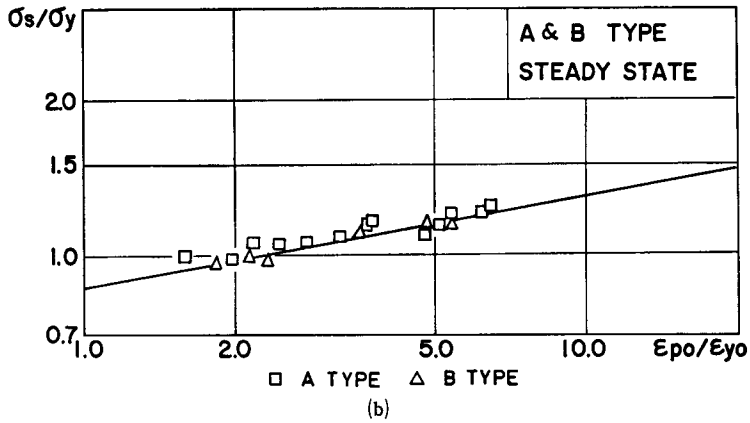
Fig. 2·24. Non-dimensional Stress and Plastic Distortion Relations at the Steady State

It can be concluded from these figures that neither the shape of the specimens nor the welding procedure influences the load–deflection curves in the initial state and the steady state. However, the cyclic hardening coefficients of the base metal differed

Fig. 2·25. Non-dimensional Absorbing Energy per Cycle and Plastic Distortion Amplitude Relations of Base Metal, A- and B-Type Specimens

from that of the welded joint which contained the steel plate stressed in the thickness direction.

4.3 Energy Absorbing Capacity

The quantitative values of energy absorping capacities of the welded beam–to–column connections may be crucial in order to assess the aseismic safety of steel structures. In Ref. 1, the authors suggested that no deterioration of the butt welded joints in the e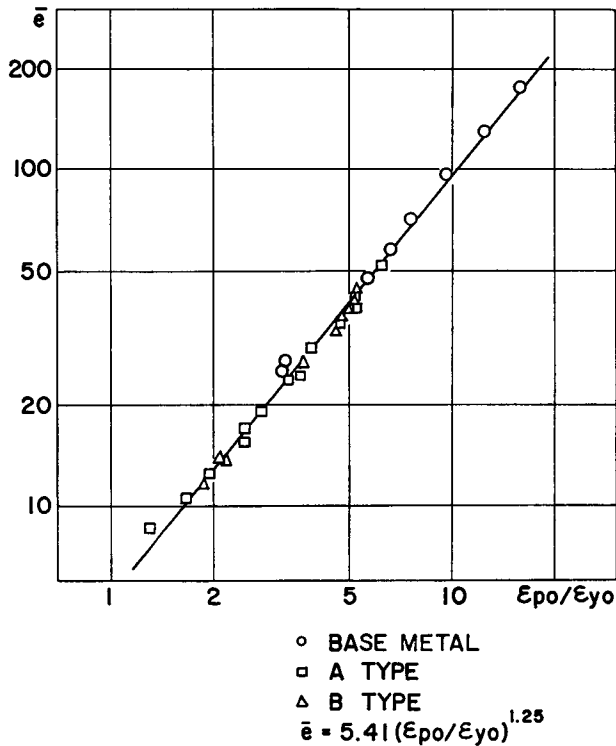nergy absorbing capacity could be found from the test results using mild or high tensile strength steels, in comparison with that of the base metals. Also, they suggested that linear relations could be formulated between the dissipated plastic strain energy and the plastic strain amplitudes in the non–dimensional form.

a)   Base Metal, and A– and B–type Specimens

In this experiment, the same method as that reported in Ref. 1 was applied to evaluate the energy absorbing capacity. The dissipated plastic energy per cycle was normalized by dividing the area of the load–deflection hysteresis loop at the steady

C-TYPE

□ − n ≒ 0.2

△ − n ≒ 0.4

◇ − n ≒ 0.6

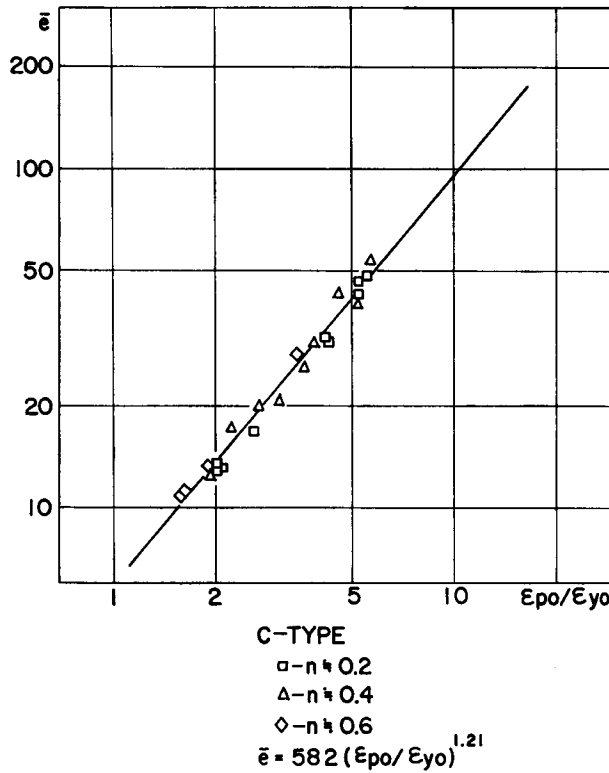$\bar{e} = 582 \, (\varepsilon_{po}/\varepsilon_{yo})^{1.21}$

Fig. 2·26.   Non-dimensional Absorbing Energy per Cycle and Plastic
Distortion Amplitude Relations of C-Type Specimens

state by the initial elastic energy $(1/2 \cdot \sigma_y \cdot \varepsilon_{y0})$. This was notified as $\bar{e}$. The non–dimensional plastic distortion amplitudes for the base metal, and for the A– and B–type specimens were calculated in the same manner as previously described in Section 4. 1.

These data are plotted on a log–log scale as shown in Fig. 2·25. Since we can not find any distinct difference between the base metal and the welded joints, the linear regressions method was adopted for all experimental data in Fig. 2·25, and the following equation was formulated:

$$\bar{e} = 5.\ 41 \left(\frac{\varepsilon_{p0}}{\varepsilon_{y0}} \right)^{1.25} \tag{9}$$

b) C–type Specimens

Fig. 2·26 shows the relation between the absorbing energy and the plastic average distortion amplitude for the C–type specimens. This figure, in which the notation n signifies the ratio of the applied column force to the yield compression load, suggests that the energy absorbing capacity of the welded beam–to–column joints is independent of the quantity of the column axial force. The relation may be expressed as follows:

$$\bar{e} = 5.\ 82 \cdot \left(\frac{\varepsilon_{p0}}{\varepsilon_{y0}} \right)^{1.12} \tag{10}$$

4.4 Fatigue Strength based upon the Outputs of Distortion Amplitudes

It was assumed that the "modified Manson–Coffin relationship" could be applied to the equivalent fatigue lives N'_f and the non–dimensional elastic and plastic distortion amplitudes $\varepsilon_{e0}/\varepsilon_{y0}$ and $\varepsilon_{p0}/\varepsilon_{y0}$, respectively. These were derived from the outputs of the extensometers at the steady states. (See Ref. 1).

a) A– and B–type Specimens

Log–log plots were made as shown in Fig. 2·27(a) and (b). From these figures, it may be tentatively concluded that a linear relationship exists among $\varepsilon_{e0}/\varepsilon_{y0}$, $\varepsilon_{p0}/\varepsilon_{y0}$ and N'_f. However, it should be noted that these figures indicate two different relationships among the test results on the A– and B–type specimens. Namely, the fatigue strengths of the A–1 and A–4 type specimens are inferior to those of the A–2, A–3, and the B–type specimens in these log–log diagrams.

As to the reason for this phenomenon, in the case of welding with back run or "non-gas arc" welding with comparatively few passes, it may be conjectured that the material had hardened and become brittle due to the weld heating.

By applying the linear regressions method to these figures, the following equations can be formulated:

For the A–1 and A–4 type specimens:

$$\frac{\varepsilon_{e0}}{\varepsilon_{y0}} = 1.\ 20 \cdot (N'_f)^{-0.10}$$

$$\frac{\varepsilon_{po}}{\varepsilon_{yo}} = 21.5 \cdot (N_f')^{-0.46} \tag{11}$$
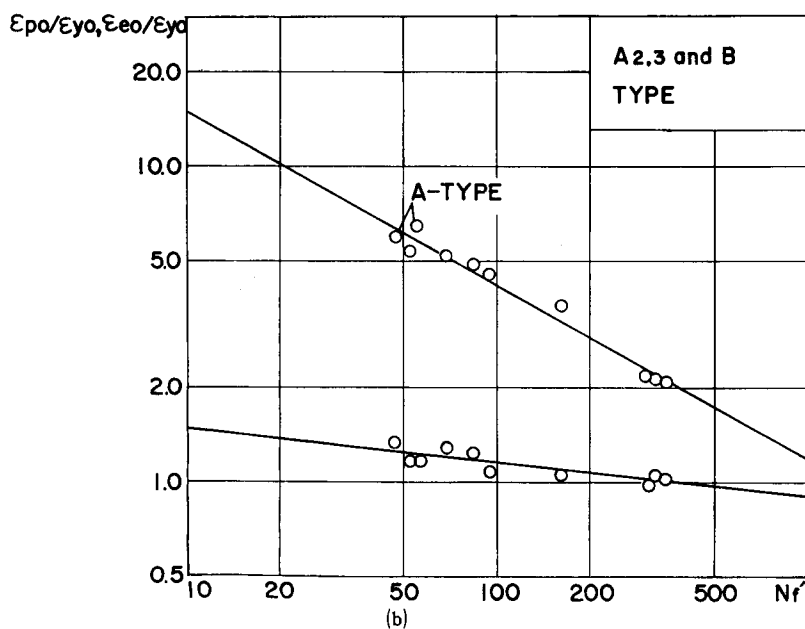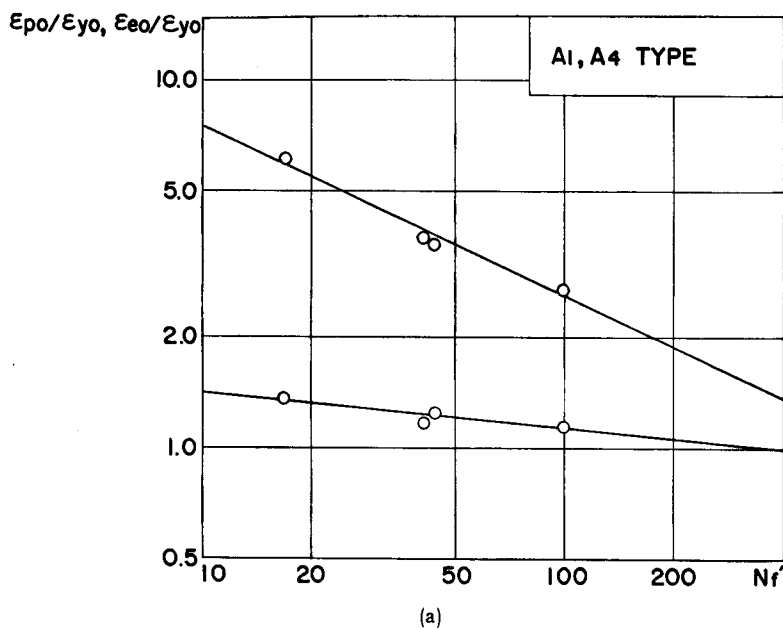

(a)

(b)

Fig. 2·27. Non-dimensional Distortion Ampitude and Fatigue Lives
Relations of A- and B-Type Specimens

$$\frac{\varepsilon_{e0}}{\varepsilon_{y0}} = 1.90 \cdot (N'_f)^{-0.11}$$

$$\frac{\varepsilon_{p0}}{\varepsilon_{y0}} = 53.8 \cdot (N'_f)^{-0.55} \tag{12}$$

For the A-2 and A-3, and for the B-type specimens:

b) C-type Specimens

The non-dimensional distortion amplitudes and the equivalent fatigue lives, described in the same manner as in the above section, are plotted in the log-log scale as shown in Fig. 2·28. Eq. (12) is also shown by the dashed line in the figure.

No significant deterioration in the fatigue strength can be observed from this figure, even though the column axial forces were being subjected to the welded beam -to-column joints.
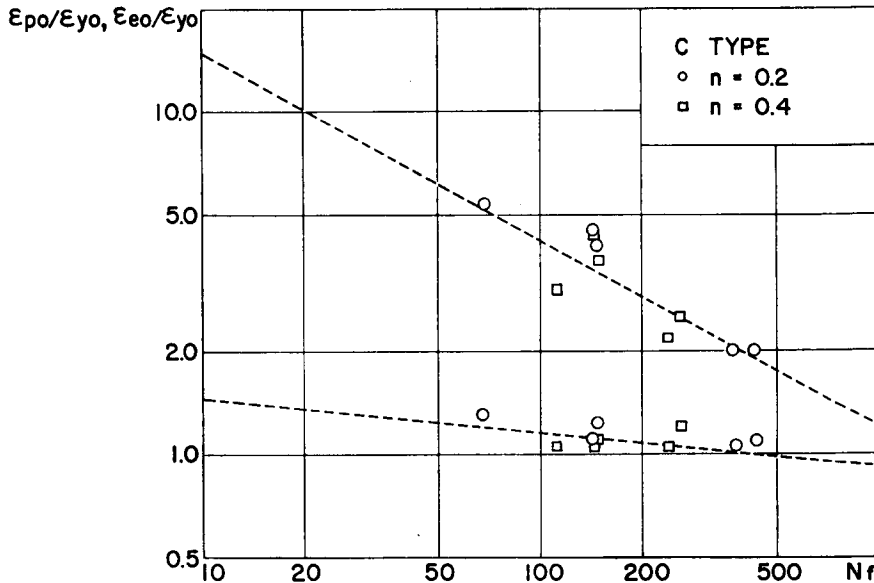

Fig. 2·28. Non-dimensional Distortion Amplitude and Fatigue Lives Relations of C-Type Specimen

5. Conclusions

From the test results examining 1) the deformation potential of the steel plates which were stressed in the thickness direction and subjected to the monotonic increasing load test, 2) the inelastic cyclic behaviors and 3) the fatigue strength of the welded beam-to-column joints, the following conclusions may be drawn:

1] It has been observed from the monotonic increasing load test that the plastic deformation capacity in the thickness direction was obviously inferior to that in the

rolling direction. The fracture surface exhibited the so-called "terrace wall". As is evident from Table 2·1, the sulphur content in the mild steel plates used in this experiment, was comparatively high, and it is observed from the test results of the through thickness directions (Table 2·3) that the values for the reduction of areas were rather low. These results agree with the test results about the susceptibility to "lamellar tearing" in experiments carried out by other investigators, such as Nagao et al[6], Kanazawa et al[7] and Nagel and Schönherr[8].

2] The overall load–deflection curves under cyclic loading do not indicate any distinct deterioration between the base metal and the welded joints containing the steel plates stressed in the thickness direction, in spite of the effects of the monotonic increasing load test and the welding procedures. In particular, a rapid convergence to stabilized hysteresis loops was clearly observed in the test results of the welded specimens. However, the shapes of the hysteresis loops, as well as the relations between the non–dimensional average stresses and the plastic average distortion amplitudes, are different at the initial state and the steady state.

3] The low–cycle fatigue strength based upon the average distortion amplitude has a significant influence upon the welding procedures, and a distinct deterioration is observed in comparison with the base metal.

4] Although the presence of the column axial force may not have an overall influence upon the shape of the hysteresis loop or the energy absorbing capacity, the local strain values of the column flanges were particularly varied under cyclic loading. Such behavior is absent under conditions free of column axial forces. From an overall viewpoint, no deterioration due to the column axial force was observed in the welded beam–to–column joint.

References

1) K. Kaneta and I. Kohzu; THIS MEMOIRS, Vol. XLIII, Part 1, Jan., p. 102 (1981).
2) T. Naka; J. of the Japan Welding Society, 24, No. 7, p. 258, and No. 11, p. 435, (1955).
3) T. Naka, B. Kato and K. Morita; The annual meeting of A.I.J., p. 899 (1968).
4) S. Ohji and S. Harada; Trans. of the Japan Society of Mechanical Engineers, 37, No. 295, p. 2193 (1972).
5) R. Hill; The Mathematical Theory of Plasticity, Oxford at the Clarendon Press, p. 317 (1950).
6) T. Nagao and H. Terasawa; J. of the Japan Welding Society, 45, No. 2, p. 31 (1976).
7) S. Kanazawa, K. Yamato, T. Inoue and K. Hashimoto; J. of the Japan Welding Society, 45, No. 2, p. 40, and No. 3, p. 72 (1976).
8) D. Nagel and W. Schönherr; Metal Construction and British Welding Journal, Feb., p. 64 (1969).